



HAL
open science

Slow Dynamics in a Semiconductor Laser Coupled to Fiber Bragg Grating

A. V. Naumenko, N. A. Loïko, Céline Guignard, Pascal Besnard

► **To cite this version:**

A. V. Naumenko, N. A. Loïko, Céline Guignard, Pascal Besnard. Slow Dynamics in a Semiconductor Laser Coupled to Fiber Bragg Grating. 11th conference on Laser Optics (LO 2003), Jun 2003, St-Petersburg, Russia. Vol.5480, pp.11-19, 10.1117/12.558452 . hal-00159357

HAL Id: hal-00159357

<https://hal.science/hal-00159357>

Submitted on 25 Apr 2022

HAL is a multi-disciplinary open access archive for the deposit and dissemination of scientific research documents, whether they are published or not. The documents may come from teaching and research institutions in France or abroad, or from public or private research centers.

L'archive ouverte pluridisciplinaire **HAL**, est destinée au dépôt et à la diffusion de documents scientifiques de niveau recherche, publiés ou non, émanant des établissements d'enseignement et de recherche français ou étrangers, des laboratoires publics ou privés.



Distributed under a Creative Commons Attribution - NonCommercial 4.0 International License

Slow dynamics in a semiconductor laser coupled to Fiber Bragg Grating

A. Naumenko^a, N.Loiko^a, C. Guignard^b, P. Besnard^b

^a Institute of Physics, National Academy of Belarus, Skorina ave., 68, 220072 Minsk, Belarus

^b ENSSAT, Laboratoire d'Optronique (UMR6082), 6 rue de Kerampont, 22305 Lannion, France

ABSTRACT

Dynamics of a semiconductor laser coupled to a fiber Bragg grating is analyzed thanks to a map, which indicates the existence of low frequency fluctuations when the reflectivity and the bandwidth of the Bragg grating are varied. The influence of these parameters is detailed and we show how the filter can be used to control the laser dynamics.

Keywords: semiconductor laser, fiber Bragg grating, Low Frequency Fluctuations

1. INTRODUCTION

A semiconductor laser subject to external optical feedback exhibits a variety of dynamical and spectral behaviors including the so-called low frequency fluctuations (LFF). The term LFF is usually applied to sudden dropouts in the averaged laser intensity. They are followed by a gradual recovery to an almost constant state of emission. The frequency of the power dropouts is much lower than the frequency of the relaxation oscillations and of the external cavity frequency.¹ This intriguing phenomenon has been widely investigated for conventional optical feedback. According to the most accepted deterministic model² based on the Lang-Kobayashi rate equations for a single-longitudinal mode semiconductor laser³ the intensity dropouts are caused by crises between local chaotic attractors and saddle-type antimodes.

In this paper, we present some results concerning LFF in the case of frequency filtered feedback. Such kind of feedback is often used in practice to obtain highly coherent source for metrology or sources for optical telecommunication. Frequency dependent feedback strength influences steady states and their stability.⁴⁻⁶ It follows that there is a possibility to control laser dynamics as it was shown for a Lorentzian filter.^{4,7} From another point of view, filtered feedback allows to get additional informations about the link that exist between the steady states set and the dynamics. In particular, the influence of the number of modes (number, which is reduced by the filter) on the LFF dynamics can be understood. Though the main tendency was described in Ref. 4 when the filter bandwidth is decreased, some aspects, for example, such as the influence of feedback level, were not studied. In this paper, the external reflector is a fiber Bragg grating and the existence and properties of LFF are carefully described when the bandwidth and the reflectivity of the filter are varied. This systematic study enables to draw a map summarizing the possibility to obtain LFF with filtered optical feedback.

2. MODEL EQUATIONS

A schematic view of the extended laser system is shown in Figure 1. The active medium is placed between two mirrors for which the amplitude reflection coefficients are r_1 and r_2 . We suppose that the solitary laser is a single mode device. The external cavity is formed by the output-mirror of reflectivity r_2 and by an external Bragg mirror of reflectivity $r_{Bragg}(\omega)$, where ω is the laser frequency. To study the dynamics of such a coupled laser, we have used a previously developed model^{5,6}:

Further author information: (Send correspondence to P.Besnard)
E-mail: pascal.besnard@enssat.fr

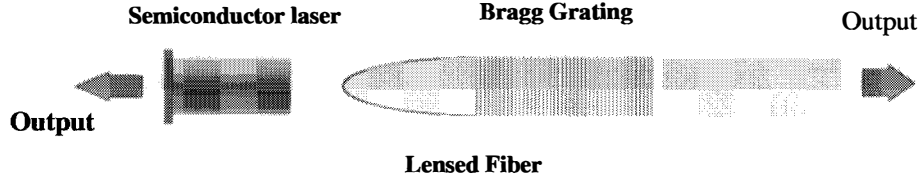


Figure 1. Schematic view of diode laser coupled to fiber Bragg grating.

$$\begin{aligned}\dot{E} &= \left[\frac{1}{2} \Gamma G_N \{ i \alpha_H (N - N_{th}) + g(N, I) \} - \frac{1}{2\tau_{ph}} + \frac{1}{\tau_{in}} \ln(F/E) \right] E, \\ \dot{N} &= \frac{J}{eV} - \frac{N}{\tau_N(N)} - G_N g(N, I) I,\end{aligned}\quad (1)$$

where the feedback terms corresponding to the influence of the external Bragg reflector can be written as:

$$\begin{aligned}F(t) &= E(t) + \frac{(-1)(1-r_2^2)}{2\pi r_2^2} \sum_{n=1}^{\infty} \exp(-i\omega_0 n\tau) \int_{-\infty}^{+\infty} d\omega (-r_2 r_{Bragg}(\omega))^n \times \\ &\times \exp(i\omega(t-n\tau)) \int_{-\infty}^{+\infty} dt' E(t') \exp(-i\omega t').\end{aligned}\quad (2)$$

Here $E(t)$ is the slowly varying complex amplitude of the laser field at time t , $E(t) = \sqrt{I(t)} \exp(i\varphi(t))$, where $I(t)$ is the laser field intensity and $\varphi(t)$ is the phase. The optical field is $E_{opt}(t) = \text{Re}(E(t) \exp(i\omega_0 t))$, where ω_0 is the optical frequency of the solitary laser and can be considered simply as the frequency of reference. The nonlinear gain is expressed by $g(N, I) = \frac{(N-N_0)}{1+\epsilon I}$, where ϵ is the gain compression factor. $N(t)$ is the carrier density, N_0 , its value at transparency, and N_{th} , at threshold: $N_{th} = N_0 + \frac{1}{\Gamma G_N \tau_{ph}}$. G_N is the differential gain, Γ is the field confinement factor. The photon lifetime τ_{ph} is determined by the full losses of solitary laser: $\frac{1}{\tau_{ph}} = \Gamma_{ph} = v_g \alpha_{in} + \frac{1}{\tau_{in}} \ln\left(\frac{1}{R_1 R_2}\right)$, where the parameter α_{in} determines the scattering losses in active volume, $v_g = c/n_D$ is the group velocity, c is the speed of light in vacuum, n_D is the group index of the active medium. Parameters R_1 and R_2 are the power reflectivity of left and right facets: $R_{1,2} = r_{1,2}^2$. The cavity lifetime is $\tau_{in} = 2L_D/v_g$ and L_D is the laser diode length. α_H is the linewidth enhancement factor, J is the injection current, e is the electron charge. The spontaneous emission rate $\frac{N}{\tau_N(N)} = AN + BN^2 + CN^3$ with A , B and C - mono-molecular, bi-molecular and Auger recombination coefficients. Linearization of the spontaneous emission rate near N_{th} gives $\frac{N}{\tau_N(N)} = \frac{N}{\tau_e} + \frac{J_0}{eV}$, where τ_e is the carrier lifetime and J_0 is a shift of the injection current. $\tau = 2L_{ext}n_{ext}/c$ is the external cavity round-trip time, where L_{ext} is the external cavity length and n_{ext} is the refraction index. $r_B(\omega)$ is the Bragg grating reflectivity at the frequency ω :

$$r_B(\omega) = -\varrho \sinh\left(L_B \sqrt{\varrho^2 - \delta^2}\right) / \left(\sqrt{\varrho^2 - \delta^2} \cosh\left(L_B \sqrt{\varrho^2 - \delta^2}\right) + i\delta \sinh\left(L_B \sqrt{\varrho^2 - \delta^2}\right)\right), \quad (3)$$

where ϱ is the complex strength of the Bragg grating, L_B is the length of the fiber Bragg grating. 2δ is the difference between the wave vectors of the incident and of the reflected fields: $2\delta = 4n_B\pi/\lambda_0 - 2\pi/\Lambda_B = (2n_B/c)(\omega_0 - \omega_B) = 2(n_B/c)\Delta\omega$, where n_B is the effective index of the Bragg grating fiber, Λ_B the Bragg grating period and λ_0 the wavelength associated to the optical frequency ω_0 . $\Delta\omega$ is the detuning from the Bragg

frequency ω_B associated to the Bragg wavelength $\lambda_B = 2n_B\Lambda_B$. Note that in the numerical simulations, the frequency is referenced to ω_0 (only deviations from this frequency are considered). The reflectivity at the Bragg wavelength (null detuning) takes the usual form: $r_B(\omega_B) = \tanh(\varrho L_B) (\simeq \varrho L_B$ for small reflectivity). In further calculations we will use the following definitions for the coupling constant κ and the bandwidth Δ of the Bragg reflector: $\kappa = \varrho L_B$, $\Delta = \frac{c}{L_B n_B} \sqrt{\pi^2 - (\kappa L_B)^2}$, ($\simeq \frac{\pi c}{n_B L_B}$).

Terms with fixed n in expression (2) for feedback $F(t)$ correspond to contributions from the n^{th} external cavity round trip. At a given value of r_B , the amount of necessary round trips is determined automatically for an accurate calculation of the feedback effect. In order to calculate the feedback term $F(t)$ and to decrease the time of calculation we use the Green function approach developed in our previous works.^{5,6} In accordance with it, the Green function of n^{th} order, $G_n(x)$, represents the n^{th} round-trip time-response of the external cavity, to a δ - functional perturbation. This function is written as:

$$G_n(x) = -\frac{1-r_2^2}{r_2^2} \exp(-i\omega_0 n\tau) \frac{1}{2\pi} \int_{-\infty}^{+\infty} d\omega (-r_2 r_B(\omega))^n \exp(i\omega x). \quad (4)$$

Then the contribution from the n^{th} round trip in the sum (2) is given by:

$$F_n(t) = \int_0^{+\infty} dx E(t - n\tau - x) G_n(x), \quad (5)$$

and the whole term describing optical feedback to the fiber Bragg grating, is given by:

$$F(t) = E(t) + \sum_{n=1}^{\infty} F_n(t). \quad (6)$$

The global parameters used in our simulations are given in the table.

Table 1. Table of parameters.

parameter	description
$V_D = 1.1 \times 10^{-16} \text{ m}^3$	volume of solitary laser
$G_N = 3 \times 10^{-20} \text{ m}^2$	differential gain
$N_0 = 1.5 \times 10^{24} \text{ m}^{-3}$	transparency carrier density
$\alpha_{in} = 800.0 \text{ m}^{-1}$	scattering losses
$\Gamma = 0.08$	field confinement factor
$\tau_e = 0.8 \text{ ns}$	spontaneous carrier lifetime
$\alpha_H = 4$	linewidth enhancement factor
$R_1 = 0.32$	reflectivity of left facet
$R_2 = 0.32$	reflectivity of right facet
$\tau_{in} = 8 \text{ ps}$	cavity life time
$L_{ext} = 0.3 \text{ m}$	external cavity length
$n_{ext} = 1.5$	effective index of the fiber

3. STEADY-STATE SET

The system dynamics depends on the new set of steady states and on their stability. These questions were considered in details in our previous work.^{5,6} It is worth to remind here the main results of this analysis.

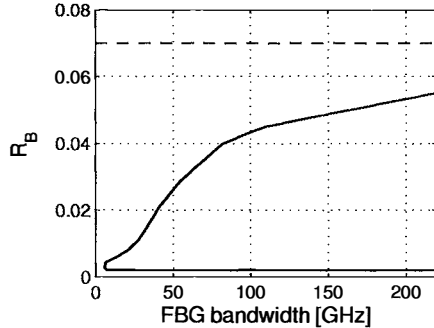


Figure 2. Domain of LFF existence.

Thus in the case of comparatively weak feedback, the steady states lie on a closed curve (almost an ellipse) in the chart frequency - intensity ($\Omega - I$). The upper branch consists of nodes (external cavity modes) and the lower branch consists of saddle steady states (antimodes). For a rather wide bandwidth of the Bragg reflector $\Delta \gg \Omega^* = (1 - r_2^2) \frac{r_B^{max}}{r_2} \frac{1}{\tau_{in}} \sqrt{1 + \alpha^2}$ (here $r_B^{max} = r_B(\omega_B)$), steady-states frequencies are within the interval: $-\Omega^* \leq \Omega_s \leq \Omega^*$. This case corresponds totally to the usual external feedback without filtering. The Free Spectral Range for the external-cavity modes is equal approximately to $\frac{2\pi}{\tau}$. The steady state which is the most stable, is the mode with maximal gain.⁸ It is located on the left (red) side of the ellipse. When the bandwidth of the Bragg grating is decreased, the ellipse containing the steady states becomes narrower and the frequency of the maximal gain mode (MGM) tends to zero. For narrower Bragg grating bandwidth and moderate feedback level, the shape of steady-state curve looks like a convex rhomb. There is also formation of satellite branches. They contain the steady states corresponding to lobes in the reflectivity of the Bragg grating. It was shown also that under strong feedback conditions new branches of solutions appear.

External cavity modes may lose stability via a Hopf bifurcation. Then regular pulsations appear. The occurrence of supplementary bifurcations leads to more complex behaviors. In the case of conventional feedback, LFF as described by deterministic model of Lang and Kobayashi, reveal the walk of the system towards the stable high-gain external-cavity mode through jumps among a serie of attractors centered on unstable external cavity modes, each of them having a higher gain than the previous one. When the system's trajectory comes too close to an anti-mode, it is expelled into another region of the phase space with lower gain modes and then the process is repeated. Obviously, the fact that the Bragg grating modifies the topology of the steady-states set, must influence the existence domain of LFF.

4. LFF DOMAIN

Figure 2 illustrates, in the Bragg grating parameter space (reflectivity- spectral bandwidth), a mapping which shows roughly the region of existence of LFF for parameters given in the table. The upper boundary of this region declines with a decrease of the spectral width and there are no more LFF when the bandwidth is lower than 7 GHz. The domain is shifted up with an increase of the pump.

It is worth noting that the existence of such a domain depends critically on values of the linewidth enhancement factor. Thus, for $\alpha_H = 3$, the corresponding domain was obtained in a very small interval of values of the pump (1 - 2% above the threshold value, at $\tau = 5$ ns). In comparison with the previous case, its extension along R_B -axis is considerably narrower (about in four times for a bandwidth 100 GHz). Stabilization of dynamics with decreasing of α_H was shown also in the case of conventional optical feedback.^{9,10}

When the operating point in the LFF domain is scanned, characteristics of LFF-regime are modified. We have observed the following scenarios of transformation of the dynamics when the Bragg-grating parameters are changed:

1) when reflectivity increases for rather wide filter bandwidth, LFF appears after distortion of coherence collapse, which transforms to regular LFF, then vanishes for strong feedback level by collision with the maximal gain mode;

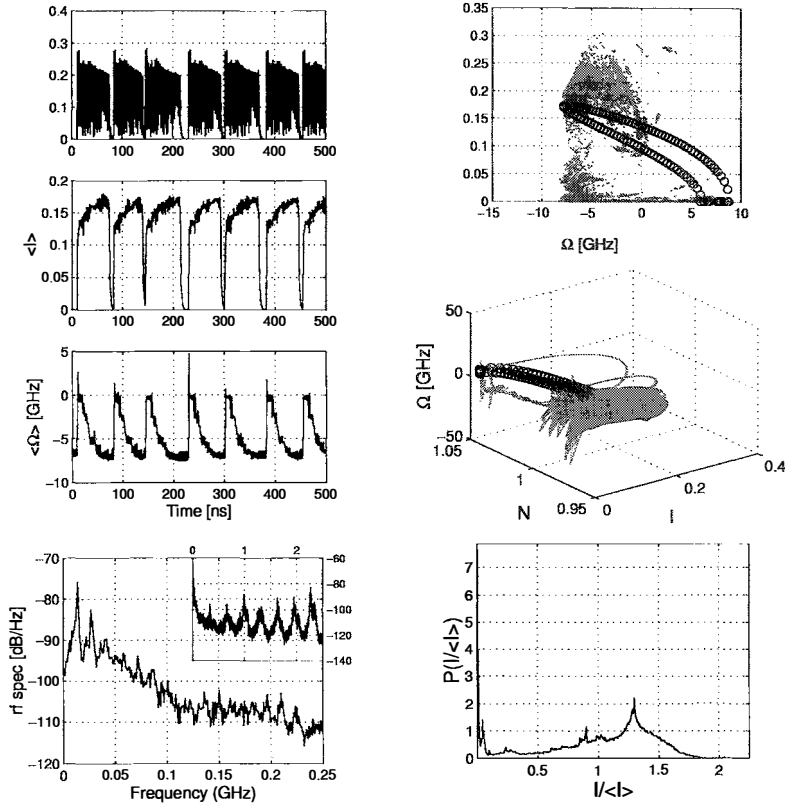


Figure 3. LFF characteristics for $2\Delta = 0.6 \text{ nm}$ (82 GHz), $R_B(\omega_B) = 0.01$.

- 2) when the filter bandwidth is decreased for rather high feedback level, the system converges to a stable steady state (through crisis and transient LFF);
- 3) finally when the bandwidth is decreased for, this time, a rather small Bragg grating reflectivity, LFF disappears via intermittent-like behavior to regular oscillations. In the following we consider the different dynamics in connection with the corresponding modification of the steady states set.

5. LFF REGIMES

To study the modification of LFF when the Bragg-grating parameters are changed, we will consider the following variables:

- a) the laser intensity vs time;
- b) the intensity averaged over 1 ns;
- c) the field frequency averaged over 1 ns;
- d) the corresponding Poincaré section (maxima of intensity) where the steady states set will be represented;
- e) the system trajectory around the steady states in 3-dimensional phase space;
- f) the radio-frequency spectrum;
- g) the probability distribution of intensity.

Typical examples of these characteristics are presented in Figures 3-7. Traces on the left charts correspond to intensity (a), averaged intensity (b), averaged frequency (c), radio frequency spectrum (f). Curves on the right correspond to Poincaré section (d), trajectory in phase space (e) and to the probability distribution (g). The integration was initialized at a mode with low gain to put the system into a LFF regime.

The parameters of Figure 3 correspond approximately to the center of LFF region for moderately wide filter. Here, we observe LFF with pronounced and almost regular dropouts, which reach almost the zero intensity

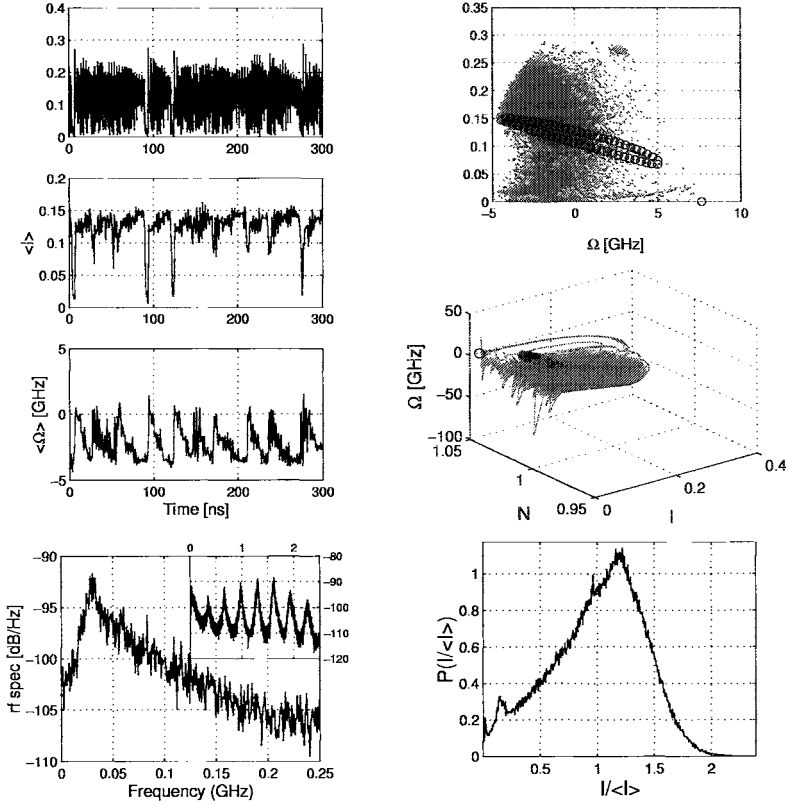


Figure 4. LFF characteristics for $2\Delta = 0.6 \text{ nm}$ (82 GHz), $R_B(\omega_B) = 0.003$.

level, with a period of 75 ns and is followed by recovery processes. The peak nearest to zero frequency in the rf-spectrum, shows the corresponding frequency of LFF dropouts. A close look to the Poincaré section shows that external cavity modes lying in the lower part of the steady-states ellipse, do not satisfy lasing conditions so that the ellipse is cut by the zero intensity level. Phase trajectory spends most of the time near the upper part of the ellipse (near the modes of highest gain), and also stays for rather long time near the zero intensity level. Heteroclinic loop, which connects these two regions, is evident in the phase space. In accordance with this behavior, the probability distribution of intensity has two pronounced maxima, corresponding to states where the system stays longer. It differs from known probability distribution,^{11,12} which was maximum near the mean intensity and was strongly asymmetric.¹¹ This last property was explained by longitudinal multimode laser operation. On the contrary, the probability density given in Ref. 12 displayed a peak at low intensity. It rolls off at several times the average intensity for both single mode and multimode cases. These experimental results were confirmed by the numerical simulations using an extension of Lang-Kobayashi equations. However, as shown,¹² the coexistence of LFF with a stable external cavity mode, leads to the appearance of a strong peak near the average intensity. It corresponds to the stable emission state, which is superposed onto the background of the exponentially decaying LFF distribution. Finally, at certain pump levels, an increase of the gain compression factor leads to a shift of the maximum towards the average intensity. This fact is not surprising as this term is known to have a stabilizing effect on the dynamics which means a tendency to force the system to operate on the stable mode. Further study is necessary to detail the conditions for coexistence of LFF and stable modes and to clarify the influence of the spontaneous emission noise.

A decrease of the feedback level puts the system closer to the lower boundary of LFF region (Figure 4). The steady-states ellipse is reduced and is not cut anymore. Thus the system spends less time near the zero intensity. The maximum of the probability density, which is close to 0 almost disappears. LFF are less regular.

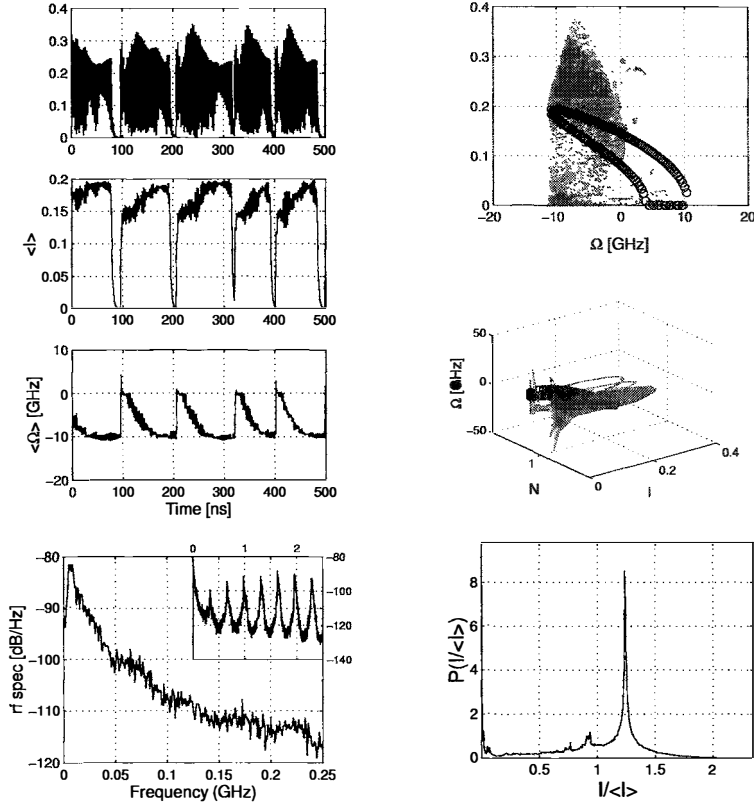


Figure 5. LFF characteristics for $2\Delta = 0.6 \text{ nm}$ (82 GHz), $R_B(\omega_B) = 0.025$.

In the same time, the second maximum of the probability distribution becomes wider. It confirms the existence of irregular pulsations involving almost all unstable modes. The system trajectory covers practically the whole steady-states set with random visits of a trivial state vicinity. The heteroclinic loop is still visible in Figure 4. We observe much more irregular oscillations which are closer to a coherence collapse regime. Nevertheless, averaged intensity and frequency (averaged period $\approx 25\text{ns}$) show that the dropouts still exist, however, they are irregular and not pronounced. For smaller values of the Bragg grating reflectivity, the steady-states ellipse is further reduced and located far from the trivial solutions (zero intensity). Dropouts disappear and the system displays a full developed coherence collapse.

If the feedback level is still increased for the same bandwidth, so that the system is put near the upper boundary of the existence region of LFF, the LFF period increases (Figure 5) as well as the number of external-cavity modes. This last results is in agreement with the known dependence of the LFF period on the number of modes.¹³ The peak in distribution density becomes narrower and sharper and it corresponds to the MGM. In other words, the system stays longer near the MGM. For stronger feedback, trajectory collides with the MGM and LFF transforms into a transient. This scenario is similar to a crisis of heteroclinic orbit. In the case of conventional optical feedback, a further increase of the feedback level may force the system to produce LFF again. It is then due to the creation of a new pair of steady states along with a loose of stability of the MGM.¹⁰ The filtered feedback in our case limits the number of steady states stabilizing the emission at a considerably low level of feedback in comparison with the classification done in Ref. 14 for conventional feedback. In order to get LFF at a strong feedback, a certain threshold value of the pump current has to be reached.

Collision of the LFF with the MGM is also observed when the filter width is decreased for comparatively strong feedback. However, here, the underlying reasons explaining this collision are not the same as the previous one. As shown in Figure 6, narrowing the filter reduces the number of external cavity modes. Moreover, it

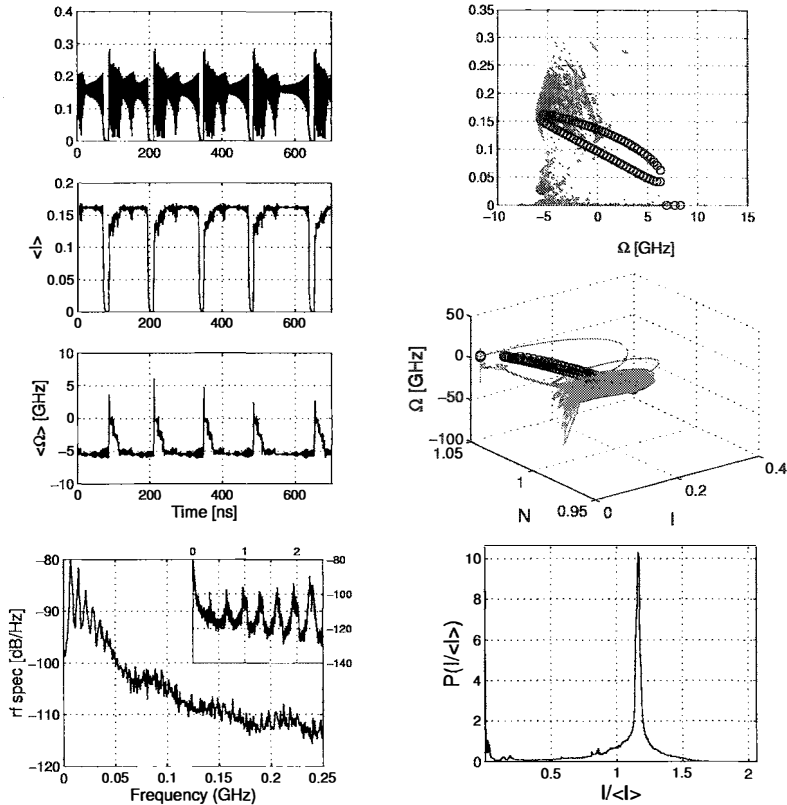


Figure 6. LFF characteristics for $2\Delta = 0.2 \text{ nm}$ (27 GHz), $R_B(\omega_B) = 0.01$.

stabilizes some of them. Slope in the upper part of the ellipse is decreased, which means a small gain difference between adjacent modes. Therefore, the system stays longer near modes with high gain. It follows an increase of the LFF period and the probability distribution shows even sharper peak for the MGM than in Figure 5.

For sharper filter, at rather weak feedback levels, the system is close to the intersection point of the two boundaries of the existence domain of LFF. As shown in Figure 7, some kind of intermittency is observed. The number of external cavity modes is strongly decreased. The system stays a very long time in the vicinity of modes with highest gain (it is a laminar phase of the system motion). The system switches between these modes and the switchings correspond to short irregular chaotic pulsations for the instant intensity. It is not comparable to the pronounced short dropouts for the averaged intensity encountered before. A further decrease of the bandwidth leads to regular dynamics. Some of them is similar to the ones presented in Ref. 4 for a Lorentzian filter.

6. CONCLUSION.

In this report, filtered optical feedback is considered using a fiber Bragg grating. Theoretical analysis and simulation has been done thanks to a previously developed theoretical model.^{5,6} We present for what we think the first time a mapping in the Bragg grating parameter space (spectral width - reflectivity) showing the region of existence of LFF. Upper boundary of this region declines with a decrease of the spectral width. LFF exist for bandwidths greater than 7 GHz when the feedback delay is equal to 3 ns. Moreover, we present detailed scenarios of changes in the LFF dynamics. Their transformation into another regime is analyzed when the Bragg reflectivity or the filter width are varied. A suppression of LFF occurs via intermittency when the width of the filter attained a narrow limit. With an increase of the reflectivity, LFF appears after a distortion of coherence collapse. It vanishes at strong feedback by collision with a stable steady state. If the feedback level is further

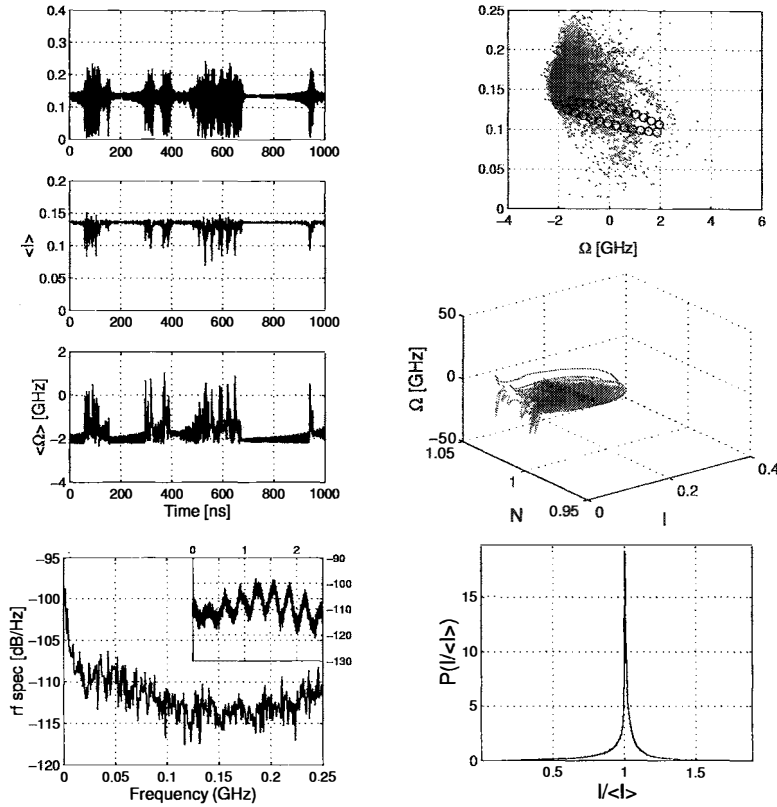


Figure 7. LFF characteristics for $2\Delta = 0.05 \text{ nm}$ (7 GHz), $R_B(\omega_B) = 0.003$.

increased, one should increase the pump current above a threshold value in order to recover the LFF regime as it is the case for conventional feedback.

REFERENCES

1. C. Risch, C. Vourmard, *J. Appl. Phys.* **48**, p.2083, 1977.
2. T. Sano, *Phys. Rev. A* **50**, p.2719, 1994.
3. R. Lang and K Kobayashi, *IEEE J. Quantum Electron.* **16**, p. 347, 1980.
4. M. Yousefy, D. Lenstra, *IEEE J. of Quantum Electron.* **35**, pp.970, 1999.
5. P. Besnard, A. Naumenko, N. Loiko, G. Ughetto, J.C. Bertreux, in *ICNO 2001: Nonlinear Optical Phenomena and Nonlinear Dynamics of Optical System*, Konstantin N. Drabovich, Nikolay S. Kazak, Vladimir A. Makarov, Alexander P. Voitovich, Editors, *Proceedings of SPIE* **4751**, p.577, 2002.
6. A. Naumenko, P. Besnard, N. Loiko, G. Ughetto, J.C. Bertreux, *IEEE J. of Quantum Electron.* (accepted for publication).
7. M. Yousefy, D. Lenstra, G. Vemuri, A. Fischer, *IEE Proc.-Optoelectron.* **148**, p. 233, 2001.
8. A.M.Levine, G.H.M. van Tarnwijk, D.Lenstra, and T.Erneux, *Phys. Rev. A* **55**, pp.R3366-R3439, 1995.
9. T. Heil, I. Fischer and W. Elsässer, *J. Opt.B: Quantum Semiclass. Opt.* **2**, p.413, 2000.
10. R.L. Davidchack, Y.-Ch. Lai, A. Gavrielides, V. Kovanis, *Physica D* **145**, p.130, 2000.
11. G. Huyet, S. Hegarty, M. Giudici, B. De Bruyn and J.G. McInerney, *Europhys. Lett.* **40**, p.619, 1997.
12. D.W. Sukow, T. Heil, I. Fischer, A. Gavrielides, A. Hohl-AbiChedid and W. Elsässer, *Phys. Rev. A* **60**, p.667, 1999.
13. G. Huyet, P.A. Porta, S.P. Hegarty, J.G. McInerney and F. Holland, *Opt. Commun.* **180**, p.339, 2000.
14. R.W. Tkach and A.R. Chraplyvy, *IEEE J. Lightwave Technol.* **4**, p. 1655, 1986.